Received: 22 March 2023 | Revised: 18 April 2023 | Accepted: 3 May 2023

DOI: 10.1002/kin.21653

INTERNATIONAL JOURNAL OF CHEMICAL KINETICS WILEY

RESEARCH ARTICLE

Theoretical kinetics analysis of the OH + CH_3OH hydrogen abstraction reaction using a full-dimensional potential energy surface

Joaquín Espinosa-Garcia | **Moisés Garcia-Chamorro**

Área de Química Física and Instituto de Computación Científica Avanzada, Universidad de Extremadura, Badajoz, Spain

Correspondence
Joaquín Espinosa-Garcia, Área de Química Física and Instituto de Computación Científica Avanzada, Universidad de Extremadura, 06071 Badajoz, Spain.
Email: joaquin@unex.es

Funding information
Junta de Extremadura and the European Regional Development Fund, Spain, Grant/Award Number: GR21032

Abstract

Based on an analytical full-dimensional potential energy surface (PES), named PES-2022, fitted to high-level ab initio calculations previously developed by our group and specifically developed to describe this polyatomic reactive process, an exhaustive kinetics analysis was performed in the temperature range 50–2000 K, that is, interstellar, atmospheric and combustion conditions. Using the competitive canonical unified theory with multidimensional tunneling corrections of small curvature, CCUS/SCT, and low- and high-pressure limit (LPL and HPL) models, in this wide temperature range we found that the overall rate constants increase with temperature at T > 300 K and T < 200 K, showing a V-shaped temperature dependence, reproducing the experimental evidence when the HPL model was used. The increase of the rate constant with temperature at low temperatures was due to the strong contribution of the tunneling factor. The title reaction evolves by two paths, H_2O + CH_2OH (R1) and H_2O + CH_3O (R2), and the branching ratio analysis showed that the R2 path was dominant at T < 200 K while the R1 path dominated at T > 300 K, with a turnover temperature of ~260 K, in agreement with previous theoretical estimations. Three kinetics isotope effects (KIEs), $^{13}CH_3OH$, $CH_3{}^{18}OH$, and CD_3OH, were theoretically studied, reproducing the experimental evidence. The kinetics analysis in the present paper together with the dynamics study previously reported showed the capacity of the PES-2022 to understand this important chemical process.

KEYWORDS
OH + CH_3OH reaction, potential energy surface, theoretical kinetics study

1 | INTRODUCTION

The study of reactions of the hydroxyl radical with alcohols is very interesting in combustion (high temperatures), atmospheric (low temperatures) and interstellar (cold temperatures) conditions. In the atmosphere there are over 70 alcohols from anthropogenic or biogenic emissions[1] and their reactions with hydroxyl radicals represent the major loss process for alcohols during daytime.[2] In the present study, we focus attention on the gas-phase

hydrogen abstraction reaction with the first species of the series, methanol, which evolves by two paths: OH attacks the CH_3 group (R1 path) or the OH group (R2 path) of methanol through a common reactant complex (RC), both paths producing water molecules,

$$OH + CH_3OH \rightarrow RC \begin{cases} \nearrow SP1 \rightarrow PC1 \rightarrow H_2O + CH_2OH & (R1) \\ \searrow SP2 \rightarrow PC2 \rightarrow H_2O + CH_3O & (R2) \end{cases}$$

where SP and PC mean the respective saddle point and product complex for each path. In this two-step model the first step, from reactants to the reactant complex, is the association or complexation process. In a previous study[3] we developed a full-dimensional potential energy surface (PES), PES-2022, simultaneously describing both paths. This surface is a valence bond and mechanic molecular functional fitted to high-level ab initio calculations at the coupled-cluster singles, doubles and perturbative triples-F12 explicitly correlated level. While in that paper[3] we focused on the dynamics description of the system (reaction cross section, product scattering distribution, product roto-vibrational distribution, etc.) in the present paper we are interested in the kinetics analysis: rate constants, branching ratios and kinetic isotope effects, and their temperature dependence.

The title reaction has been widely studied, both experimentally (an exhaustive review can be found in the NIST[4] and the GRI-mech[5] kinetics databases) and theoretically,[6–18] where the rate constants and their temperature dependence show contradictory results. Figure 1A shows the experimentally found temperature dependence of the overall rate constants in the wide temperature range 10–2000 K, where only five studies reported values at T < 100 K,[17,19–22] in the low-temperature interstellar environment, and most of the experimental works have focused on the range 200–2000 K.[4,5] A clear smoking pipe-shape in the Arrhenius plot, or in brief, V-shaped dependence, was observed with a minimum of about 200 K, which suggests a change of mechanism with temperature. Today, there is some consensus that the R2 path becomes dominant at low temperatures, T < 200 K, where the quantum mechanical tunneling effect represents the main contribution, while at T > 300 K the R1 path is the main channel, although this consensus has varied over time. In the low-temperature interstellar regime, Shannon et al.[19] in 2013 reported surprisingly large rate constants using a pulsed Laval-nozzle apparatus with flash photolysis, two orders of magnitude larger than at 200 K, due mainly to the role of tunneling, where the CH_3O branching ratio is 99% at 70 K. Subsequent studies in the regime of cold and ultra-cold temperatures[17,20–22] have confirmed these conclusions.

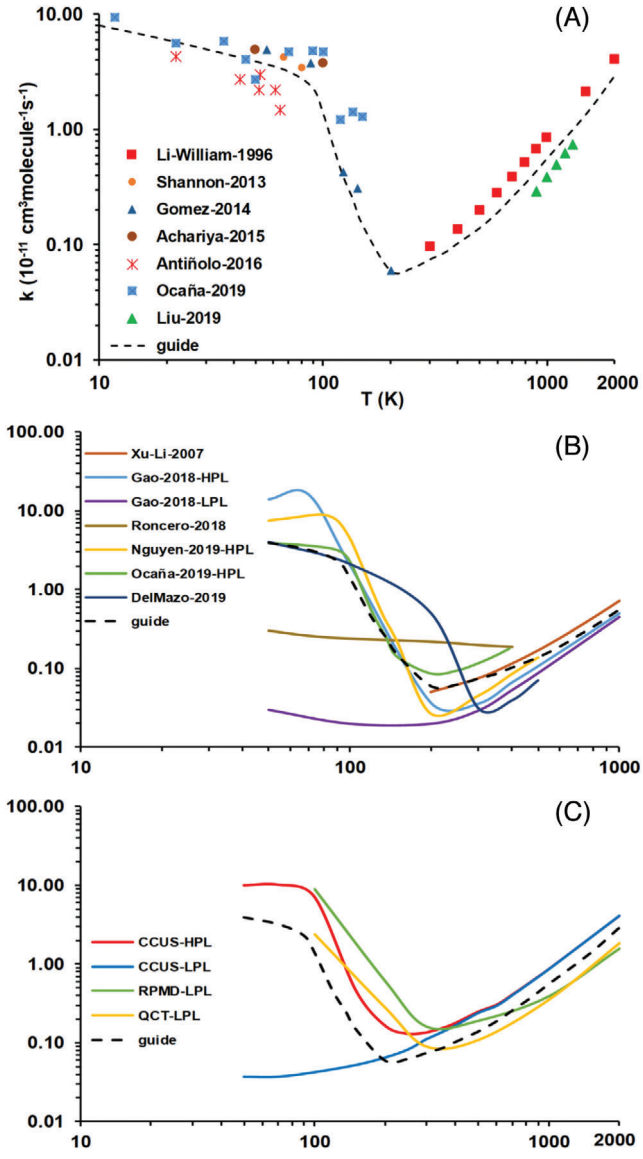

FIGURE 1 Panel (A) Overall experimental rate constants of the OH + CH3OH reaction at temperatures from 10 to 2000 K.[17–25] The black dashed line is used only as a guide to the eye. Panel (B) Overall rate constants from representative theoretical results from literature.[9,12–17] Panel (C) overall rate constants from present work, using different kinetics tools on PES-2022 surface.

With respect to the independent rate constants on the two paths, the experimental information is scarce, where both paths presented dispersion of values, larger in the case of the R2 path. For the R1 path, in 1981 Vandooren and Van Tiggelen[23] analyzed the kinetics at high temperatures, 1000–2000 K, proposing the expression

$$k(T) = 7.97 \times 10^{-11} \left[\text{cm}^3/\text{molecules}\right] e^{-18.79[\text{kJ/mole}]/RT}$$

The GRI-mech database[5] and Li and Williams[24] in 1996, in a wider temperature range 300–2500 K, proposed the

expression,

$$k(T) = 2.39 \times 10^{-18} [cm^3/^{molecule}s] T^{2.00} e^{0.200[kJ/mole]/RT}$$

and recently, Liu et al.[25] in 2019 reported the following expression in the high temperature regime 900–1300 K,

$$k(T) = 2.55 \times 10^{-11} \left[cm^3/molecules\right] e^{-19.02[kJ/mole]/RT}$$

where in the common 1000 K temperature, for instance, the rate constant presented discrepancies, $8.32.10^{-12}$, $3.65.10^{-12}$ and $2.59.10^{-12}$ cm^3 $molecule^{-1}s^{-1}$, respectively, that is, a factor greater than two. For the R2 path, the experimental information is also scarce and presents larger discrepancies.[5,24–27] In 1984, Warnatz[27] reported an exhaustive review of the previous literature for the R2 path in the temperature range 300–2000 K,

$$k(T) = 1.66 \times 10^{-11} \left[cm^3/molecules\right] e^{-7.10[kJ/mole]/RT}$$

with k(1000 K) = $7.07.10^{-12}$ cm^3 $molecule^{-1}s^{-1}$; while the GRI-mech database[5] and Li and Williams[24] in 1996, in a wider temperature range 300–2500 K, proposed the expression,

$$k(T) = 1.045 \times 10^{-17} \left[cm^3/molecules\right] T^2 e^{-0.358[kJ/mole]/RT}$$

and more recently Liu et al.[25] in the high temperature range 900–1300 K, reported the expression

$$k(T) = 4.3 \times 10^{-11} \left[cm^3/molecules\right] e^{-28.79[kJ/mole]/RT}$$

with a value at 1000 K of $1.35.10^{-12}$ cm^3 $molecule^{-1}s^{-1}$, that is, five times lower. In addition, the two first experimental measures presented different temperature dependence, that is, different slopes of the Arrhenius representations. With respect to the $R2/R_{TOTAL}$ branching ratio, experimental values at room temperature between 10%–25% were reported,[28,29] although its temperature dependence presented contradictory results.[24,25]

Theoretically, the title reaction has received much attention, where both the R1 and R2 paths have been independently analyzed[3,6–18] using different electronic structure calculations, ab initio and density functional theory, DFT. The most recent and accurate calculations used the coupled-cluster with single, double and triple (perturbative) excitations, CCSD(T), a level based on optimized geometries at lower levels. These theoretical results showed that both the R1 and R2 paths present large exothermicity, in reasonable agreement with the experimental measures from the corresponding standard enthalpies of formation,[30,31] $\Delta H_R{}^o(298K) = -22.74 \pm 0.08$ and -13.62 ± 0.08 kcal mol^{-1}, respectively. These studies showed a common reactant complex in the reactant channel, stabilized with respect to the reactants, and product complexes in the exit channel, also stabilized with respect to the respective products, $H_2O + CH_2OH$ for the R1 path and $H_2O + CH_3O$ for the R2 path. The barrier heights, a sensitive parameter in the kinetics analysis, presented values in the range 0.8–1.5 for the R1 path and 3.6–4.0 kcal mol^{-1} for the R2 path. The corresponding imaginary vibrational frequencies characterizing the saddle points and directly related with the tunneling effect also presented a wide range of values from the literature[3,8–10,12] showing that it is a property difficult to describe: 437 i-1420 i cm^{-1} for the R1 path and 1737 i-2958 i cm^{-1} for the R2 path. However, Nguyen et al.[16] concluded that "In this case, at least, CCSD(T) does not appear to be enough". For the title reaction, two analytical PESs[3,13] have been reported using different strategies. Roncero et al.[13] reported the first global PES for this reaction, which is based on ~200 000 ab initio points obtained at the CCSD(T)-F12 explicitly correlated method using a basis set of quality double-zeta, and developed as a many-body (MB) expression. This surface gives barriers of 2.1 and 6.7 kcal mol^{-1}, respectively, that is, overestimating the literature information, especially for the R2 path, while the corresponding imaginary vibrational frequencies were, respectively, 1576 i and 2263 i cm^{-1}, where the value for the R1 path seems overestimated. Recently, our group developed a new surface, PES-2022,[3] which is an analytical full-dimensional surface developed as a combination of valence bond and molecular mechanic functional (VB/MM), fitted to high level ab initio calculations at the CCSD(T)-F12 explicitly correlated level using a basis set of quality triple-zeta. The corresponding barrier heights and imaginary frequencies are, respectively, 1.42 kcal mol^{-1} and 858 i cm^{-1} for the R1 path, and 3.66 kcal mol^{-1} and 2176 i cm^{-1} for the R2 path, reproducing the high-level ab initio data used in the fitting and the most accurate values from literature, which lends confidence to the new PES-2022 surface. In our previous paper[3] based on PES-2022 we performed an exhaustive dynamics study using quasi-classical trajectory (QCT) calculations. When comparison with experiment was possible,[32] this PES reasonably simulated the experimental evidence.

In the theoretical analysis, different kinetics tools have been used in the literature: conventional transition state theory,[8] variational transition state theory,[9] competitive canonical unified statistical model,[12] QCT calculations,[13] ring polymer molecular dynamics (RPMD),[14] combined two-dimensional master-equation/semi-classical transition state theory/variational Rice-Ramsperger–Kassel–Marcus approach,[16] etc. In general, the temperature dependence of the preferred mechanism of reaction, R1 or R2 path, and of the rate constants were very sensitive to the tool used. The first studies focused on medium and high

temperatures, T > 200 K with different results. So, while Jodkowski et al.[7] overestimated the experimental rate constants, Galano et al.[8] underestimated them. Xu and Lin[9] in 2007 found a good agreement with experiment, and similar results were reported by Gao et al.[12] The theoretical branching ratios showed contradictory results in this temperature regime. Galano et al.[8] in the temperature range 290–500 K and Xu and Lin[9] in a wider temperature range, 200–3000 K, reported that R1 > R2 in all the temperature regimes. However, Gao et al.[12] reported that R1 dominates at high temperatures (T > 150 K or T > 300 K, depending on the model used, LPL or HPL) while R2 is the preferred mechanism at lower temperatures. These latter results agree with Shannon et al.[19] who used a master equation predicting a turnover temperature of ~250 K and with the recent results from Nguyen et al.[16]: R2 dominates at low temperatures (T ≤ 50 K) while R1 dominates at high temperatures (T ≥ 200 K).

In the present theoretical work, we present an exhaustive kinetics analysis based on PES-2022. Three different kinetics tools were used: variational transition-state with multidimensional tunneling corrections, VTST/MT, RPMD, RPMD, and QCT calculations, QCT. The present paper is organized as follows. The PES[3] is briefly described in Section 2, together with the kinetics computational details using VTST/MT, RPMD, and QCT approaches. In Section 3, we present the kinetics results obtained in the present work, comparing them with the experimental evidence and previous theoretical results. Finally, the main conclusions are summarized in Section 4.

2 | THEORETICAL TOOLS

To describe this polyatomic reactive system, in a previous work[3] we developed a full-dimensional PES, PES-2022. Basically, this surface is a valence-bond/molecular mechanics (VB/MM) analytical function fitted to a reduced number of high-level ab initio calculations at the CCSD(T)-F12/aug-cc-pVTZ level. It simultaneously describes both the attack of the OH radical on the CH_3 of methanol (R1 path) and on the OH of methanol (R2 path) and presents an average root mean square error of 0.7 kcal mol^{-1}. This surface was subjected to a series of stringent tests in order to analyze its quality and versatility to describe, in a smooth and continuous way, the topology of this reactive system from reactants to products. In the previous work[3] this surface was used in an exhaustive dynamics analysis, comparing the dynamics results with the experimental evidence. In general, when comparison was possible, PES-2022 reasonably simulated the experiments in dynamics properties as varied as product energy partitioning, products roto-vibrational distributions or products scattering distributions, which represented a stringent test of its quality.

In the analysis of the overall experimental rate constants (Figure 1A) a V-shaped temperature dependence was clearly observed, where at T < 200K the R2 path was dominant and at T > 300 K the dominant path was R1, as well as a pressure dependence. The pressure dependence is difficult to analyze theoretically and is beyond the scope of the present work. Gao et al.[12] in the transition-state theory frame proposed two limiting cases: low- and high-pressure limits, LPL and HPL, respectively. In the first case, the reaction was considered as a direct bimolecular hydrogen abstraction reaction, where the participation of the reactant complex was ignored; while in the second case, the reactant complex was fully stabilized, playing an important role, and so the overall reaction was considered as a two-step process: (i) a bimolecular association reaction from the reactants to the reactant complex, k_a, followed by (ii) an unimolecular hydrogen abstraction reaction from the reactant complex to products passing through the respective transition state, $k_{H,1}$ and $k_{H,2}$ for the R1 and R2 paths, respectively. For both the LPL and HPL models, following the suggestion of Gao et al.,[12] in the present paper the rate constants were calculated using the competitive canonical unified theory, CCUS,

$$k_i^{CCUS} = \frac{k_a}{k_{a+k_{H,1}+k_{H,2}}} k_{H,i} \quad (1)$$

Different approaches can be used to calculate the association coefficient, k_a: (i) the hard-sphere collision model,[12] which is based on van der Waals diameters of reactants; (ii) Georgievskii and Klippenstein's model,[33] which is based on dipole-dipole reactants interactions, or (iii) Gorin's model,[34–36] which is based on topology considerations, that is, fitting of the model to the PES-2022 information. In the present paper we used the Gorin model, which is a simple approach based on an attractive PES,

$$V_{MEP} = -\frac{C_6}{R^6} \quad (2)$$

where R is the distance between the two approaching reactants and C_6 is a parameter to fit the model to the PES-2022 surface, which in this case has a value of $56.34.10^{-79}$ J m^3. In this model, the rate constant is given by

$$k^{Gorin}(T) = k_a = \left(\frac{\pi}{\mu}\right)^{\frac{1}{2}} (2K_BT)^{\frac{1}{6}} \Gamma\left(\frac{2}{3}\right) C_6^{1/3} \quad (3)$$

where μ is the reduced mass and $\Gamma(2/3)$ is the incomplete Γ function. In the range 50–2000 K the rate constants are

very fast, in the order of 10^{-10} cm^3 molecule^{-1}s^{-1}. Note that this data is of a similar order to that obtained with the other two approaches.[12,37]

Next, we calculated the hydrogen abstraction rate constants for the R1 and R2 paths, $k_{H,1}$ and $k_{H,2}$, using the canonical variational transition state theory (CVT) with the small tunneling approach (SCT), CVT/SCT,[38]

$$K_{H,i}(T) = \sigma_{ik}^{CVT}(T)\, k^{SCT}(T) \quad (4)$$

where σ_i is the symmetry number accounting for the degeneracy of the reaction path, $k^{CVT}(T)$ the canonical variational rate constant and $\kappa^{SCT}(T)$ the tunneling correction. In TST-based methods the treatment of anharmonicity of frequencies and mode-mode coupling is challenging in polyatomic systems and here we consider the harmonic oscillator and rigid rotor models. Depending on whether the model is LPL or HPL, the largest difference for the rate constant calculation is the way to obtain the tunneling contribution. In the LPL model the reactant complex is unreachable (the reactants cannot be stabilized by collisions) and therefore a direct bimolecular reaction occurs. In this case, we consider the sum of the ground-state energies of the reactants as the lowest energy at which tunneling correction is considered. However, in the HPL model, the reactant complex is stabilized and now the lowest energy for the tunneling contribution corresponds to the ground-state energy of the reactant complex. Finally, note that in this kinetics analysis a multi-surface factor, defined as the ratio between the electronic partition functions of the transition state and reactants, is considered,

$$f = \frac{Q_{el}^{\neq}}{Q_{el}^{R}} = \frac{2}{2 + 2\exp(-\varepsilon/k_B T)} \quad (5)$$

where the number 2 in the numerator corresponds to the transition state, in which the spin-orbit coupling is assumed to be fully quenched, and the denominator corresponds to the electronic partition function of the OH reactant, where $\varepsilon = 140$ cm^{-1} for the OH radical.[39]

As an additional test of the capacity of the analytical PES-2022 surface to describe the kinetics of the title reaction, two other kinetics tools were used: RPMD[40–44] and QCT calculations, which presented some difficulties in the present study. In the case of RPMD, firstly, because it is a kinetics approach for bimolecular reactions and therefore can only be applied in the LPL approach. In fact, del Mazo et al.[14] performed a study of the title reaction using the RPMD approach, reporting that the lifetimes of the complex in the entrance channel are long, and comparable to the time scale of the tunneling process. Due to the quantum effects, zero-point energy (ZPE) and tunneling, this complex can be formed at zero pressure (zero pressure limit, ZPL), concluding that RPMD calculations (which capture these quantum effects) on the ZPL model are equivalent to variational transition state theory, VTST, assuming the HPL model. Therefore, in the present work and for a direct comparison with the previously analyzed CCUS-HPL method, we used the RPMD method on the LPL model, in the temperature range 100–2000 K, calculating the rate constants independently for each reaction path, R1 and R2. The second difficulty arose because the computational effort increases when temperature decreases, that is, a larger number of beads are necessary for convergence. For instance, del Mazo et al.[14] used 96, 128, 192, 384, and 768 beads at temperatures of 500, 300, 200, 100, and 50 K, respectively. The computational effort at $T \leq 100$ K is beyond our computational capacity. Therefore, in the temperature range analyzed in the present work we used 4, 8, 32, 64, 128, and 128 beads at temperatures of 2000, 1000, 500, 300, 200, and 100 K, respectively. Obviously, this smaller number of beads will determine the convergence and this point will be analyzed later. In the case of QCT, the difficulties appear due to its classical nature and therefore its application at low temperatures is questionable due to the tunneling contribution, a determinant factor in the title reaction. In the present study, QCT calculations were performed for comparison with the other kinetics approaches, independently for each reaction path, R1 and R2. At each temperature, 2000, 1000, 500, 300, 200, and 100 K, we used 10^5, 10^5, 2×10^5, 10^6, 10^6, and 10^6 trajectories, respectively, with the following maximum impact parameter, 4.0, 4.2, 5.1, 6.1, 6.6, and 7.2 Å, respectively. The C-OH (R1 path) or the O-OH (R2 path) separation was fixed at 15.0 Å, with a propagation step of 0.1 fs. The QCT approach presents two important limitations: the zero-point energy (ZPE) violation problem, and the non-consideration of tunneling contribution. With respect to the first problem, when all trajectories were considered the rate constants were overestimated, and to minimize this problem, in the present work a passive method was used, where only the reactive trajectories with product vibrational energies (H_2O and CH_2OH/CH_3O) above their respective ZPEs were considered (DZPE, double zero-point energy, approach). With respect to the second problem, the tunneling correction was included in the QCT rate constants as obtained with the SCT-LPL model. Obviously, these two approaches are very crude and the QCT rate constants are reported in this case only for a direct comparison of methods. Finally, note that in both RPMD and QCT corrected results the multi-surface factor, Equation (5), was included. In consequence, here these two approaches are used in order to test the CCUS rate constants and the PES-2022 when compared with experiments. In the kinetics

analysis the following codes were used: POLYRATE2016,[45] RPMDrate[46] and VENUS96.[47]

3 | KINETICS RESULTS

3.1 | Rate constants

In the literature, theoretical and experimental rate constants are frequently presented together in the same Figure for comparison. This is a good option when the kinetics tendencies are similar (and the available information is scarce), but when the behaviors diverge (and the available information is abundant) this presentation may mask the comparison. Therefore, in the present paper we chose to dissect the presentation of the results for a more adequate comparison. Figure 1 shows the overall rate constants for the title reaction, that is, the sum of the R1 and R2 paths. In panel (A) the experimental overall rate constants are plotted in the temperature range 10–2000 K.[17–25] Note that the experimental measures do not correspond to a single study, but are the result of several experimental groups and conditions, that is, no group has studied the overall temperature range. From the combination of experimental studies, a clear V-shaped dependence with temperature is observed with a minimum of about 200 K. Today, there is an experimental consensus that (i) at temperatures above the turnover temperature R1 is the dominant path, while at temperatures lower, the R2 path dominates due to a great contribution of the tunneling effect and (ii) these studies suggest a pressure dependence of the rate constants, although Ocaña et al.[17] reported that no dependence was observed below 100 K. Panel (B) presents some representative theoretical results from the literature,[9,12–17] in the temperature range 50–1000 K. In order to analyze pressure dependence, two limiting situations were considered: low- and high-pressure limits, LPL and HPL, respectively. In the first case, the reaction can be considered as a direct hydrogen abstraction reaction, while in the second case, the reaction evolves through a complex in the entrance channel, which is stabilized with a population of energy states in accordance with a Boltzmann distribution. In panel (B) firstly, one observes a dispersion of theoretical results, for instance, with differences of three orders at 100 K and a factor of only two at 1000 K. Secondly, while the LPL model[12] underestimated the rate constants, especially at low temperatures, using the HPL model, Gao et al.,[12] Ocaña et al.,[17] and Nguyen et al.[16] reasonably simulated the experimental behavior, with the best agreement obtained by Ocaña et al.[17] Using their own MB-PES surface, Roncero et al.[13] reported rate constants in poor agreement with experiment, with a negligible temperature dependence in the range 50–400 K. Panel (C) shows the theoretical results from the present work, using different kinetics tools. The CCUS-HPL model simulates the V-shaped dependence with temperature experimentally observed, while the CCUS-LPL model underestimates this tendency at low temperatures. This behavior, for both HPL and LPL models, agrees with the results obtained by Gao et al.[12] using different PESs.

In order to complete the kinetics analysis of the title reaction we also analyzed the behavior of the RPMD and QCT tools. In the temperature range, 100–2000 K, the RPMD and QCT results also showed the experimental V-shaped temperature dependence. As noted in the previous section, the RPMD and QCT calculations assumed the LPL model, and the minimum temperature was obtained ~300 K, larger than with the CCUS-HPL model. As previously noted, lower temperatures ($T < 100$ K) cannot be reported by computational limitations and the differences with respect to the CCUS model and/or experiments are due to convergence problems in the RPMD approach or the estimation of tunneling corrections in the QCT approach. This comparison between different kinetics tools permits us to conclude that CCUS/SCT results assuming the HPL model are equivalent to RPMD and QCT results on the LPL model, in accordance with the conclusions of del Mazo et al.[14]

In sum, the PES-2022 surface showed its ability to represent this reactive system, and the differences with experiment are due to limitations of the kinetics tools used and/or computational limitations from our group.

Obviously, the overall rate constants previously analyzed are the sum of the rate constants for each path, R1 + R2. Let us now analyze these components in an independent way (Figure 2). We begin by analyzing the R1 path, left column of Figure 2, which is the dominant path at high temperatures. In panel (A) the experimental rate constants are plotted in different temperature ranges.[5,23–25] While Li and Williams[24] presented results in the temperature range 300–2000 K, Vandooren and Van Tiggelen[23] and Liu et al.[25] reported only results at high temperatures, 1000–2000 K. In the common 1000 K temperature, the experimental values show differences of a factor two. In panel (B) the theoretical rate constants obtained in the present work using different kinetics tools on the PES-2022 surface are presented in a wider temperature range, 200–2000 K, together with other representative theoretical results[7–9,12] for comparison. In general, all theoretical results show a similar tendency with temperature, although obviously the absolute values present discrepancies, with differences of a factor of about seven at 200 K and of about five at 2000 K. The present kinetics results, using different kinetics tools, CCUS-HPL, CCUS-LPL, RPMD-LPL and QCT-LPL, on the PES-2022 surface, present an intermediate

INTERNATIONAL JOURNAL OF CHEMICAL KINETICS WILEY

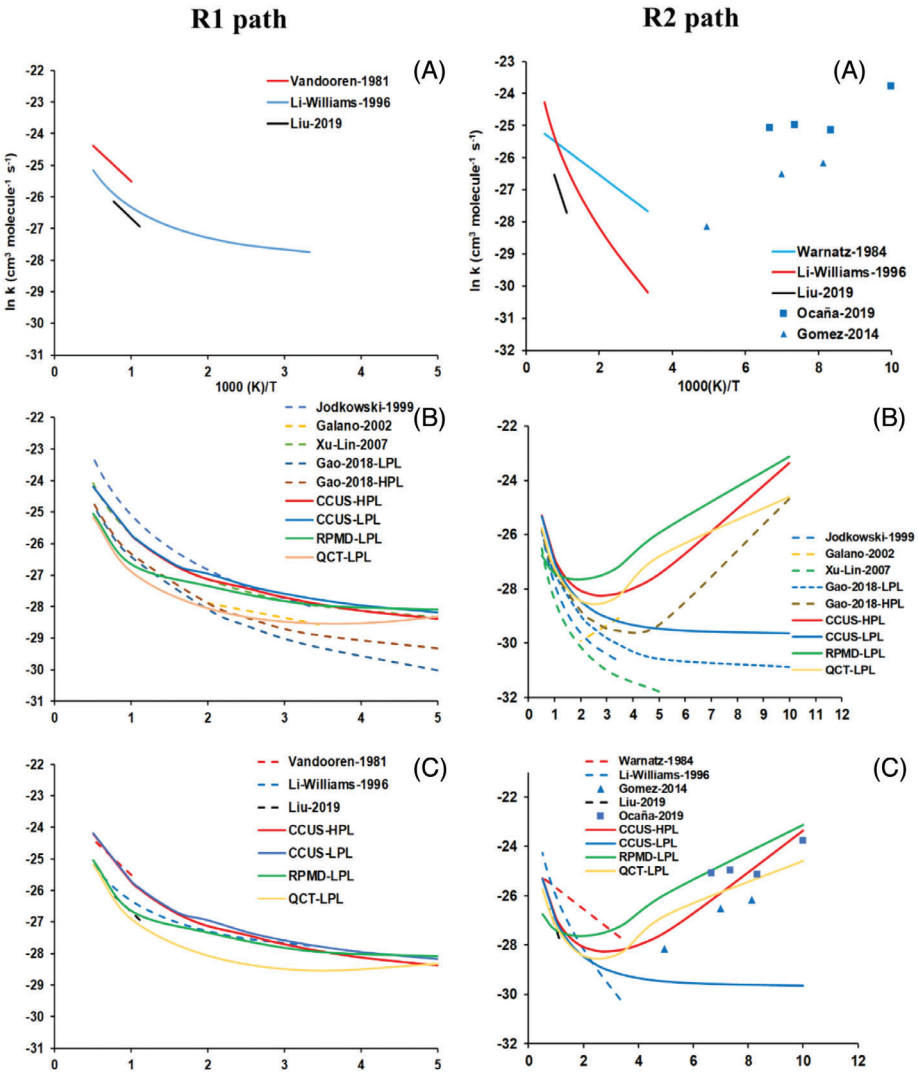

FIGURE 2 Arrhenius plots of the OH + CH_3OH thermal rate constants. Left column, R1 path, and right column, R2 path. In each column, Panel (A) Experimental rate constants from Refs.[5,17,20,23,24,25,27]; Panel (B) Theoretical rate constants from the present work computed using PES-2022 and CCUS, RPMD and QCT methods together with other representative theoretical results from Refs.[7–9,12]; Panel (C) Experimental and theoretical thermal rate constants from the present work for a direct comparison.

behavior, although the QCT-LPL results show a pronounced curvature. Finally, in panel (C) we plot the theoretical results obtained in the present work together with the experimental evidence for a direct comparison. In general, our results simulated reasonably well the experimental evidence for the R1 path, in the common temperature range. As previously noted, at high temperatures the differences between the HPL and LPL models were negligible. In consequence, in this temperature regime the three models used in the present work, CCUS, RPMD and QCT, gave a similar picture of the process, with the largest difference found when the QCT method (including ZPE constraints) was used, which underestimates the experiments and presents the largest curvature.

With respect to the R2 path the situation is more confusing and interesting (right column of Figure 2). Panel (A) shows the experimental thermal rate constants,[5,17,20,24,25,27] where the variation with temperature and the absolute values differs from one result to another, with a clear V-shaped temperature dependence in the 100–2000 K range and a turnover temperature of about 200 K. At 1000 K, for instance, these values differ by a factor of six while at 120 K the differences are smaller,[17,20] a factor of about three. In addition, Li and Williams's[24] values presented a more pronounced slope than the values reported by Warnatz,[27] although no group studied the overall temperature range. Theoretical rate constants obtained in the present paper using different kinetics tools on the PES-2022 surface are shown in panel (B) together with some representative theoretical results.[7–9,12] From the literature, only the results from Gao et al.[12] using the HPL model simulated the V-shaped dependence experimentally reported, while

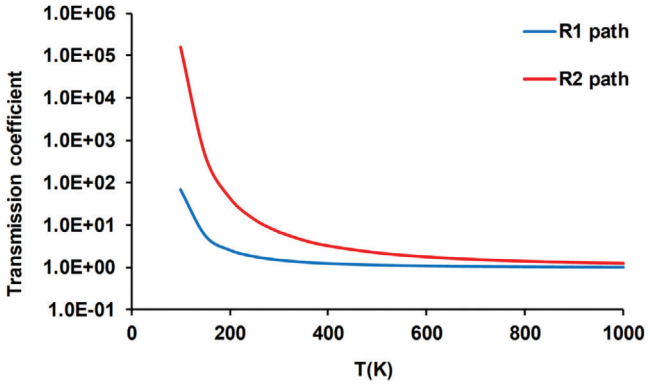

FIGURE 3 Tunneling transmission coefficients calculated using the SCT approach (HPL model) for both the R1 and the R2 paths.

the other theoretical results[7–9] did not show this dependence, which was due to the small temperature range analyzed, T > 200 K in those studies. Clearly, the LPL model[12] did not reproduce the experimental behavior. The CCUS-HPL, RPMD-LPL and QCT-LPL approaches in the present work simulated the V-shaped temperature dependence, although the turnover was found at different temperatures. The CCUS results using the LPL model (direct hydrogen abstraction reaction) does not show this dependence, being closer to the Gao's results using the LPL model.[12] Finally, the comparison of the present results with experiments is plotted in panel (C). All theoretical results reasonably simulate the experimental behavior in the 100–2000 K temperature range, except the CCUS-LPL model. The CCUS-HPL approach shows the best agreement with experiment, where the high values at T < 200 K are a consequence of the tunneling effect.

Given its importance in the title reaction, let us now analyze the tunneling contribution temperature dependence, independently for each path, Figure 3, assuming the CCUS/SCT-HPL model, which in general better simulated the experimental evidence. In this representation different behaviors of the tunneling contribution are clearly observed in both the R1 and R2 paths. The tunneling factor is larger for the R2 path, which is the cause of the V-shaped temperature dependence previously analyzed and the reason for its pre-eminence at low temperatures. At 1000 K, for instance, the R2/R1 tunneling transmission coefficient ratio is 1.23/1.04. This ratio is 6.88/1.53 at 298 K, and $1.57.10^5$/69.90 at 100 K. Obviously, this ratio increases at lower temperatures, where at 50 K it is $8.11.10^{15}$/$1.34.10^9$, that is, a difference of six orders of magnitude.

Finally, let us analyze in more detail the three kinetics approaches studied in this section. At the highest temperatures, T ≥ 1000 K, where the tunneling is absent, the overall rate constants obtained with the CCUS (HPL or LPL) approach were larger than with the RPMD or QCT approaches (which present good agreement between them) by a factor of about two. Given that the RPMD rate theory is exact[43] in the classical high-temperature regime, this result suggests that the CCUS method overestimates the rate constants, and we suggest that this behavior is related to approximations used in this theory: anharmonicity treatment of the lowest vibrational modes, which strongly affect the location of the dividing surface in the TST-based methods; mode-mode coupling or considering the reaction coordinate motion as separable. To the best of our knowledge, in polyatomic systems such as the title reaction, a general method to successfully deal with anharmonicity along the reaction path has not been proposed,[48,49] but a similar behavior was found in other hydrogen abstraction reaction,[50,51] $O(^3P) + CH_4$ and $OH + CH_4$. The QCT results, which are also immune to these difficulties, gave rate constants similar to those of RPMD. For instance, at 1000 K, the RPMD and QCT rate constants reproduced the most recent experimental measures,[25] both for the R1 and the R2 paths, which represents an indirect test of quality of the PES-2022 surface. Since the RPMD calculations at high temperatures are being used as test of quality, we also performed RPMD calculations at 2000 K using a larger number of beads, 16 rather than 4, in order to analyze their convergence. The results with 16 or 4 beads are practically the same, with differences <2%, similar in both paths. Therefore, we conclude that the RPMD calculations are converged at high temperatures. Next, the low-temperature regime is analyzed, where the quantum mechanical tunneling effect is very important. In this case, the CCUS/SCT rate constants are similar to the QCT results, due to the fact that the tunneling correction is artificially included in the QCT method, while the RPMD rate constants overestimate these values. This behavior of the RPMD approach has been previously observed for asymmetric reactions,[50–53] where the RPMD approach overestimates the exact rate constant by a factor of 2–3 in the deep tunneling regime. Furthermore, RPMD convergence problems at low temperatures cannot be discarded, because of the limited number of beads used (for instance, 128 beads at 100 K, due to our computational limitations).

3.2 | Branching ratio temperature dependence

As has been pointed out throughout the text, the experimental rate constants presented great dispersion, notable discrepancies, and the overall temperature range has not

been studied by one group under the same conditions, which makes their use as reference for comparison difficult. In this section, the branching ratio was analyzed, which represents further evidence of these discrepancies. Although all the experimental measures[24,25,28,29,54–57] coincided in that at room temperature the R2/TOTAL branching ratio was small, 10%–25%, discrepancies appeared with its temperature dependence. In general, the experimental measures were clear evidence that the CH_3O yield (R2 path) increases with temperature, except in one of the last experimental studies,[25] which reported the opposite behavior. For instance, at 1000 K, Li and Williams in 1996[24] reported an R2 branching ratio of 0.57, a crossover temperature of 800 K, and that R2 was dominant at T > 800 K; while Olm et al.[57] in 2017 reported a value of 0.30, a crossover temperature of ~1300 K, and that R2 was the dominant path at T ≥ 1300 K. These results contrast with the last experimental measure in 2018[25], where the branching ratio was 0.34 and R2 was the minority path at T ≥ 900 K. As for the theoretical studies, the situation is not clearer, although the most recent studies point in the same direction. While Galano et al.[8] (290–500 K) and Xu and Liu[9] (200–3000 K) reported that R1 > R2 in these temperature regimes, practically constant with temperature, where the R2 contribution is less than 10%, Shannon et al.[19] using a master equation reported an R2 branching ratio of 0.36 at 298 K, where the R1 path dominates at T ≥ 250 K, and Gao et al.[12] reported that R1 dominates at high temperatures while R2 is the preferred mechanism at lower temperatures. Gao et al. reported an R2 branching ratio of 0.34 at 298 K and a crossover temperature of about 200 K (depending on whether the HPL or the LPL model used), in accordance with Shannon et al.'s conclusions. In sum, no theoretical result supports the experimental conclusions about the increase of the R2 path at high temperatures, except the conclusions derived from the Liu et al.'s work.[25]

In order to shed more light on these discrepancies, Figure 4 shows the branching ratio temperature dependence obtained in the present work using the CCUS/SCT approach on the two HPL and LPL models. The LPL model does not show temperature dependence, in accordance with the theoretical results of Galano et al.[8] and Xu and Lin.[9] However, the HPL model agrees with the recent theoretical results of Shannon et al.[19] and Gao et al.[12] The turnover temperature obtained in the present work is ~260 K, in concordance with the Shannon et al.'s value, ~250 K[19] and Gao et al.'s results ~200 K.[12] We hope that the present results, together with recent theoretical studies, stimulate more experimental studies on this issue, which is of great importance in the modeling of different environments (combustion, atmospheric and interstellar chemistry).

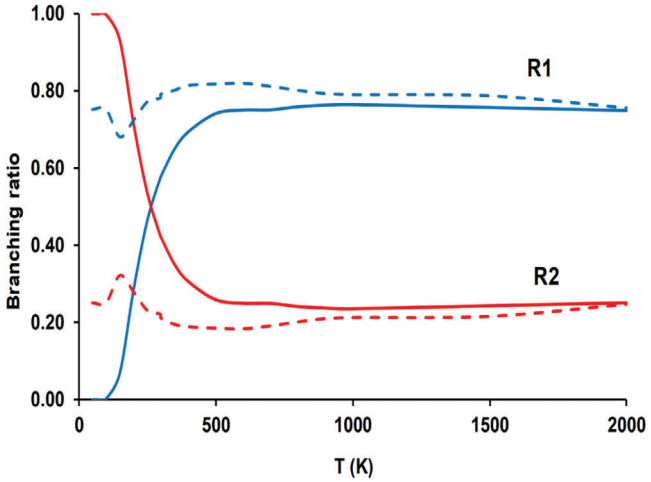

FIGURE 4 Branching fractions of the OH + CH_3OH reactions calculated in the CCUS model on the PES-2022 surface. The solid lines are for the high-pressure limit, and the dashed lines are for the low-pressure limit.

3.3 | Kinetics isotope effects

Other important kinetics magnitudes are the kinetics isotope effects (KIEs), which are defined as the ratio of the light-species rate constants (OH + CH_3OH) to the heavy-species one (OH + $^{13}CH_3OH$; OH + $CH_3{}^{18}OH$ and OH + CD_3OH). Given that the KIEs are calculated as a ratio, they are less sensitive to the accuracy of the PES and more sensitive to the kinetics tools used. In the present study, the CCUS/SCT-HPL model is used and the branching ratios for each isotope are taken into account, that is, the KIEs are given by

$$KIE = \frac{k_1^L + k_2^L}{k_1^H + k_2^H} \quad (6)$$

where the superscripts L and H mean, respectively, light and heavy species, and the subscripts correspond to the R1 and R2 paths. A point of caution is necessary in this analysis (Equation 6). The branching ratios for the OH + CH_3OH reaction were analyzed in the previous subsection. Now we compare this behavior with the tendencies for the other isotopes, Figure 5. Note that the branching ratios for the ^{13}C and ^{18}O isotopes practically mimic the OH + CH_3OH tendency, and therefore they are not represented. However, the branching ratio for the deuterated isotope, OH + CD_3OH reaction, is very different. For this deuterated reaction the R2 path is dominant at higher temperatures than for the nondeuterated isotope. In fact, while the turnover temperature for the nondeuterated isotope is ~260 K, for the deuterated isotope it is ~440 K.

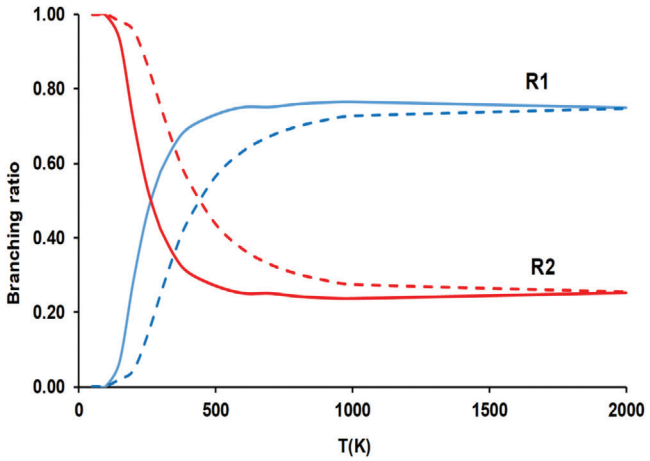

FIGURE 5 Branching fractions calculated in the CCUS-HPL model on the PES-2022 surface. The solid lines are for the OH + CH_3OH reaction, and the dashed lines are for the deuterated OH + CD_3OH reaction.

TABLE 1 Temperature dependence of the kinetics isotope effects for the OH + CH_3OH reaction.[a] CCUS/SCT-HPL values on the PES2022 surfaces, considering both the R1 and the R2 paths, Equation (6)

T(K)	^{13}C	^{18}O	CD_3OH
50	1.000	1.000	1.000
70	1.001	1.000	1.000
100	1.293	1.025	1.292
200	1.427	1.036	1.345
298	1.073	1.013	2.114
400	1.023	1.310	2.945
500	1.233	1.248	2.864
700	1.027	1.029	2.050
1000	1.021	1.010	1.688
2000	1.011	0.992	1.333

[a]At 298 K, the experimental values are, respectively: 1.031 ± 0.020, 1.017 ± 0.012, and 2.566 ± 0.042 from Ref.[10] and 2.28 for the CD_3OH isotope from Ref.[25].

Scarce experimental evidence has been reported.[10,25] Feilberg et al.[10] reported ^{13}C, ^{18}O, and D fractionation effects in the title reaction at room temperature, with KIE values of: 1.031 ± 0.020, 1.017 ± 0.012, and 2.566 ± 0.042, respectively, and Liu et al.[25] reported CH_3OH/CD_3OH KIEs at different temperatures. At 298 K, they reported a value of 2.28, in good agreement with the previous result. The calculated KIEs at 298 K in the present work are, respectively: 1.073, 1.013, and 2.114, reproducing reasonably well the experimental evidence. In addition, to complete the kinetics study Table 1 shows the variation of the three KIEs with temperature in the range 50–2000 K. At low temperatures, T < 100K, the KIEs are practically the unity for the three KIEs studied and this result agrees with the theoretical values of Gao et al.[12] As noted by these authors, this result is a consequence of the fact that the rate constants for both isotopes become equal to the association rate constants, k_a, which are practically the same in both isotopes, Equation (3), with small differences in the reduced mass.

4 | CONCLUSIONS

In this work we investigated the kinetics of the gas-phase reaction OH + $CH_3OH \rightarrow H_2O + CH_2OH/CH_3O$ in the temperature range 50–2000 K, using the competitive canonical unified statistical (CCUS) approach and the small curvature tunneling (SCT) correction to treat the barrier crossing. Pressure dependence is taken into account using two models, low- and high-pressure limits, LPL and HPL, respectively. All kinetics calculations were based on an analytical full-dimensional PES, PES-2022, previously developed in our group.

At high temperatures, T > 300 K, we found that the tunneling contribution is small or negligible and both the LPL and the HPL models present similar rate constants, the two models reasonably reproducing the experimental evidence. At lower temperatures, T < 200 K, the situation is different. We found a strong tunneling contribution, especially important for the R2 path, and while the LPL model underestimates the experimental rate constants the HPL model reasonably agrees with experimental data. In the present work, using the CCUS/SCT-HPL model we found a V-shaped temperature dependence of the overall rate constants, reproducing the experimental evidence.

We also calculated the branching ratio. While the LPL model does not present practically temperature dependence, where the R1 path is dominant ~80%, the HPL model presents a turnover temperature at about 260 K, where at lower temperatures the R2 path is dominant and at higher temperatures the R1 path dominates. This last result with the HPL model agrees with recent results from theoretical literature and they suggest a revision of the previously reported branching ratios and indeed, of the R1 and R2 rate constants dependence temperature. In view of these results, it seems that the R1 rate constants show greater convergence from several studies and we suggest that more attention should be paid to the R2 rate constants.

The KIEs are another sensitive test of the theoretical tools used, the PES and the kinetics approaches. Three KIEs, ^{13}C, ^{18}O and CD_3OH, were reported in the temperature range 50–2000 K using the CCUS/SCT-HPL model. At 298 K, the theoretical values simulated the experimental evidence. At T < 100 K, these values are practically the unity, due to the fact that the rate constants for both isotopes practically coincide with the association rate

constant, which is very fast, of the order of 10^{-10} cm^3 $molecule^{-1}$ s^{-1}.

In sum, these results show the capacity of the PES-2022 surface and the kinetics theoretical tools used to describe this polyatomic system, which is a difficult case due to the presence of a stabilized intermediate complex in the entrance channel, the presence of two different reaction paths, and the effect of the pressure. In addition, the results are highly reliant on the applied kinetic models. Finally, note that in the theory/experiment comparison many factors must be taken into account: theoretically, the kinetics approaches with their corresponding limitations, together with the accuracy and limitations of the PES, and experimentally, the quality and accuracy of the measurements. In the study of the title reaction this comparison has been complicated because of the dispersion of theoretical and experimental measures.

ACKNOWLEDGMENTS

This work was partially supported by the Junta de Extremadura and the European Regional Development Fund, Spain (Projects No. GR21032). The authors gratefully acknowledge the computer resources at Lusitania (COMPUTAEX) and technical support provided by COMPUTAEX. We are grateful to James McCue for assistance in language editing.

CONFLICT OF INTEREST STATEMENT

The authors declare no conflicts of interest.

DATA AVAILABILITY STATEMENT

The data that support the findings of this study are available from the corresponding author upon reasonable request.

REFERENCES

1. Graedel TE, Hawkings DT, Claxton LD. *Atmospheric Chemical Compounds*. Academic Press; 1986.
2. Seinfeld JH, Andino JM, Bowman FM, Frostner HJ, Pandis S. Tropospheric chemistry. *Adv Chem Eng*. 1994;19:325-405.
3. Espinosa-Garcia J, Rangel C. Analytical potential energy surface and dynamics for the OH + CH_3OH reaction. *J Chem Phys*. 2023;158:054302.
4. NIST Chemical Kinetics Database web page. Standard Reference Database 17, Version 7.0 (web version), Release 1.6.8. Data version 2015.09
5. GRI-mech Version 2.11 web page, released 9/6/1995, CHEMKIN-II format, Bowman CT, Hanson RK, Davidson DF, et al. http://combustion.berkeley.edu/gri-mech/
6. Pardo L, Banfelder JR, Osman R. Theoretical studies of the kinetics, thermochemistry, and mechanism of hydrogen-abstraction from methanol and ethanol. *J Am Chem Soc*. 1992;114:2383-2390.
7. Jodkowski JT, Rayez MT, Rayez JC, Berces T, Dobe S. Theoretical study of the kinetics of the hydrogen abstraction from methanol. 3. Reaction of methanol with hydrogen atom, methyl, and hydroxyl radicals. *J Phys Chem A*. 1999;103:3750-3765.
8. Galano A, Alvarez-Idaboy JR, Bravo-Perez G, Ruiz-Santoyo ME. Gas phase reactions of C1–C4 alcohols with the OH radical: a quantum mechanical approach. *Phys Chem Chem Phys*. 2002;4:4648-4662.
9. Xu S, Lin MC. Theoretical study on the kinetics for OH reactions with CH_3OH and C_2H_5OH. *Proc Combust Inst*. 2007;31:159-166.
10. Feilberg KL, Gruber-Stadler M, Johnson MS, Muhlhauser M, Nielsen CJ. ^{13}C, ^{18}O, and D fractionation effects in the reactions of CH_3OH isotopologues with Cl and OH radicals. *J Phys Chem A*. 2008;112:11099-11114.
11. Siebrand W, Smedarchina Z, Martinez-Nuñez E, Fernandez-Ramos A. Methanol dimer formation drastically enhances hydrogen abstraction from methanol by OH at low temperature. *Phys Chem Chem Phys*. 2016;18:22712-22718.
12. Gao LG, Zheng J, Fernandez-Ramos A, Truhlar DG, Xu XF. Kinetics of the methanol reaction with OH at interstellar, atmospheric, and combustion temperatures. *J Am Chem Soc*. 2018;140:2906-2918.
13. Roncero O, Zanchet A, Aguado A. Low temperature reaction dynamics for CH_3OH + OH collisions on a new full dimensional potential energy surface. *Phys Chem Chem Phys*. 2018;20:25951-25958.
14. Mazo-Sevillano P, Aguado A, Jimenez E, Suleimanov YV, Roncero O. Zero- and high-pressure mechanisms in the complex forming reactions of OH with methanol and formaldehyde at low temperatures. *J Phys Chem Lett*. 2019;10:1900-1907.
15. Naumkin F, Mazo-Sevillano P, Aguado A, Suleimanov YV, Roncero O. Zero- and high-pressure mechanisms in the complex forming reactions of OH with methanol and formaldehyde at low temperatures. *ACS Earth Space Chem*. 2019;3(7):1158-1169.
16. Nguyen TL, Ruscic B, Stanton JF. A master equation simulation for the •OH + CH_3OH reaction. *J Chem Phys*. 2019;150:084105.
17. Ocaña AJ, Blazquez S, Potapov A, et al. Gas-phase reactivity of CH_3OH toward OH at interstellar temperatures (11.7–177.5 K): experimental and theoretical study. *Phys Chem Chem Phys*. 2019;21:6942-6957.
18. Ali MA, Balaganesh M, Al-Odail FA, Lin KC. Effect of ammonia and water molecule on OH + CH_3OH reaction under tropospheric condition. *Scientific Reports*. Nature portfolio, 2021;11:12185.
19. Shannon RJ, Blitz MA, Goddard A, Heard DE. Accelerated chemistry in the reaction between the hydroxyl radical and methanol at interstellar temperatures facilitated by tunnelling. *Nat Chem*. 2013;5:745-749.
20. Gomez Martín JC, Caravan RL, Blitz MA, Heard DE, Plane JMC. Low temperature kinetics of the CH_3OH + OH reaction. *J Phys Chem A*. 2014;118:2693-2701.
21. Acharyya K, Herbst E, Caravan RL, Shannon RJ, Blitz MA, Heard DE. The importance of OH radical – neutral low temperature tunnelling reactions in interstellar clouds using a new model. *Mol Phys*. 2015;113(15-16):2243-2254.
22. Antiñolo M, Agúndez M, Jiménez E, et al. Reactivity of OH and CH_3OH between 22 and 64 K: modelling the gas phase production of CH_3O in Barnard 1B. *Astrophys J*. 2016;823(1).
23. Vandooren J, Van Tiggelen PJ. Experimental investigation of methanol oxidation in flames: mechanisms and rate constants of elementary steps. *Symp Int Combust Proc*. 1981;18:473-483.
24. Li SC, Williams FA. Experimental and numerical studies of two-stage methanol flames. *Symp Int Combust Proc*. 1996;26:1017-1024.

25. Liu D, Giri BR, Farooq A. A shock tube kinetic study on the branching ratio of methanol + OH reaction. *Proc Combust Inst*. 2019;37:153-162.
26. Meier U, Grotheen HH, Riekert G, Just T. Temperature dependence and branching ratio of the CH_3OH + OH reaction. *Chem Phys Lett*. 1984;106:97-101.
27. Warnatz J. *Rate Coefficients in the C/H/O System, Combustion Chemistry*. In: Gardiner WC Jr, ed. Springer-Verlag; 1984.
28. Meier U, Grotheen HH, Riekert G, Just T. Study of hydroxyl reactions with methanol and ethanol by laser-induced fluorescence. *Ber Bunsenges Phys Chem*. 1985;89:325-327.
29. McCaulley JA, Kelly JA, Golde MF, Kaufmann F. Kinetic studies of the reactions of F and OH with CH_3OH. *J Phys Chem*. 1989;93:1014-1018.
30. Ruscic B, Pinzon RE, von Laszewski G, et al. Active Thermochemical Tables: thermochemistry for the 21st century. *J Phys Conf Ser*. 2005;6:561-570.
31. Ruscic B. Active Thermochemical Tables: sequential bond dissociation enthalpies of methane, ethane, and methanol and the related thermochemistry. *J Phys Chem A*. 2015;119:7810-7837.
32. Butkovskaya NI, Setser DW. Infrared chemiluminiscence from water-forming reactions: characterization of dynamics and mechanisms. *Int Rev Phys Chem*. 2003;22:1-72.
33. Georgievskii Y, Klippenstein SJ. Long-range transition state theory. *J Chem Phys*. 2005;122:194103.
34. Gorin E. Acta Physicochim. *USSR*. 1938;9:68.
35. Garrett BC, Truhlar DG. Generalized transition state theory. Bond energy-bond order method for canonical variational calculations with application to hydrogen atom transfer reactions. *J Am Chem Soc*. 1979;101:4534-4548.
36. Rai SN, Truhlar DG. Variational transition state theory calculations for an atom – radical reaction with no saddle point: O+OH. *J Chem Phys*. 1983;79:6046.
37. Gonzalez D, Lema-Saavedra A, Espinosa S, et al. Reaction of OH radicals with CH3NH2 in the gas phase: experimental (11.7–177.5 K) and computed rate coefficients (10–1000 K). *Phys Chem Chem Phys*. 2022;24:23593-23601.
38. Fernandez-Ramos A, Ellingson A, Garrett BC, Truhlar DG. Variational transition state theory with multidimensional tunneling. *Rev Comput Chem*. 2007;23:125-232.
39. *JANAF Thermochemical Tables*. 3rd ed. National Bureau of Standards, 1998:14.
40. Craig IR, Manolopoulos DE. Quantum statistics and classical mechanics: real time correlation functions from ring polymer molecular dynamics. *J Chem Phys*. 2004;121:3368.
41. Collepardo-Guevara R, Suleimanov YV, Manolopoulos DE. Bimolecular reaction rates from ring polymer molecular dynamics. *J Chem Phys*. 2009;130:174713.
42. Collepardo-Guevara R, Suleimanov YV, Manolopoulos DE. Erratum: "Bimolecular reaction rates from ring polymer molecular dynamics" [J. Chem. Phys. 130, 174713 (2009)]. *J Chem Phys*. 2010;133:049902.
43. Suleimanov YV, Collepardo-Guevara R, Manolopoulos DE. Bimolecular reaction rates from ring polymer molecular dynamics: application to H + CH_4→ H_2 + CH_3. *J Chem Phys*. 2011;134:044131.
44. Suleimanov YV, Aoiz FJ, Guo H. Chemical reaction rate coefficients from ring polymer molecular dynamics: theory and practical applications. *J Phys Chem A*. 2016;120:8488-8502.
45. Zheng J, Bao JL, Meana-Paneda R, et al. *Polyrate-2016-2A*. University of Minnesota; 2016.
46. Suleimanov YV, Allen JW, Green WH. RPMDRATE: bimolecular chemical reaction rates from ring polymer molecular dynamics. *Comput Phys Commun*. 2013;184:833-840.
47. Hase WL, Duchovic RJ, Hu X, et al. VENUS96: a general chemical dynamics computer program. *QCPE Bull*. 1996;16(4):671.
48. Isaacson AD. Including anharmonicity in the calculation of rate constants. 1. The HCN/HNC isomerization reaction. *J Phys Chem A*. 2006;110:379-388.
49. Isaacson AD. Including anharmonicity in the calculation of rate constants. II. The OH+ H_2 → H_2O+H reaction. *J Chem Phys*. 2008;128:134304.
50. Gonzalez-Lavado E, Corchado JC, Suleimanov YV, Green WH, Espinosa-Garcia J. Theoretical kinetics study of the $O(^3P)$ + CH_4/CD_4 hydrogen abstraction reaction: the role of anharmonicity, recrossing effects, and quantum mechanical tunnelling. *J Phys Chem A*. 2014;118:3243-3252.
51. Suleimanov YV, Espinosa-Garcia J. Recrossing and tunneling in the kinetics study of the OH + CH_4 → H_2O + CH_3 reaction. *J Phys Chem B*. 2016;120:1418-1428.
52. Suleimanov YV, de Tudela RP, Jambrina PG, et al. A ring polymer molecular dynamics study on the family of isotopologues of the H + H_2 reaction. *Phys Chem Chem Phys*. 2013;15:3655-3665.
53. Richardson JO, Althorpe SC. Ring-polymer molecular dynamics rate-theory in the deep-tunneling regime: connection with semiclassical instanton theory. *J Chem Phys*. 2009;131:214106.
54. Hägele J, Lorent K, Rhäsa D, Zellner R. Rate constants and CH_3O product yield of the reaction. OH + CH_3OH → products. *Ber Bunsenges Phys Chem*. 1983;87:1023-1026.
55. Dobé S, Berces T, Temps F, Wagner HG, Ziemer H. Formation of methoxy and hydroxymethyl free radicals in selected elementary reactions. *Symp (Int) Combust*. 1994;25:775-781.
56. Hess WP, Tully FP. Hydrogen-atom abstraction from methanol by hydroxyl radical. *J Phys Chem*. 1989;93:1944-1947.
57. Olm C, Varga T, Valkó E, Curran HJ, Turanyi T. Uncertainty quantification of a newly optimized methanol and formaldehyde combustion mechanism. *Combust Flame*. 2017;186:45-64.

How to cite this article: Espinosa-Garcia J, Garcia-Chamorro M. Theoretical kinetics analysis of the OH + CH_3OH hydrogen abstraction reaction using a full-dimensional potential energy surface. *Int J Chem Kinet*. 2023;55:525–536. https://doi.org/10.1002/kin.21653